Heliyon 9 (2023) e18458

Contents lists available at ScienceDirect

Heliyon

journal homepage: www.cell.com/heliyon

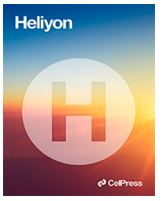

Review article

Different ways to approach shale reservoirs' CO_2 storage potential in America

Ruichong Ni *, Kegang Ling, Samuel Afari

University of North Dakota, Grand Forks, ND, USA

ARTICLE INFO

Keywords:
Shale
CO2 adsorption
CO2 storage

ABSTRACT

To achieve the Net Zero Carbon Emissions (NZCE) target by 2050, Carbon Capture, Utilization, and Storage (CCUS) is a major method. Gathering and injecting CO_2 into shale reservoirs is an effective way to reduce the CO_2 amount in the air and thus, release the greenhouse effect. CO_2 injection into organic-rich shales could provide dual benefits of incremental oil or gas recovery and secure CO_2 storage. When planning the CO_2 injection project, the most important question is how much gas could be stored in the reservoir. Methods for calculating CO_2 storage potential in shale reservoirs have been studied by many researchers. However, few researchers put those methods together and make comparisons to each other. This paper summarized five methods for evaluating CO_2 storage potential in five shale reservoirs by using the literature published in recent years. This paper aims to discuss and evaluate the technical aspects related to gas storage. Those geomechanical properties, petrophysical properties, and construction parameters were discussed. Among those parameters, CO_2 injection rate, skin factor, and Knudsen diffusion could significantly affect CO_2 storage potential evaluation results. Also, if well integrity, especially cement quality, and permeability could be taken into consideration, CO_2 storage simulation models' results will be more realistic. The significances of this study are: (1) served as guidance in calculating CO_2 storage capacity in shale oil plays; (2) provides analyses in evaluating nowadays methods' limitations; (3) gives recommendations to researchers on how to improve those methods or create a new one.

1. Introduction

Mingxing Bai et al. [1] mentioned that greenhouse gas such as CO_2 is a major villains of global warming and climatic changes. Take the United States for example, since 1970, the temperature has increased by 2.6 °F (1.4 °C) due to climate change [2]. Fig. 1 shows the rate of Temperature Change in the United States from 1901 to 2021 [3]. In 2020, 5.2 billion metric tons of carbon dioxide equivalent greenhouse gas (GHG) emissions were produced by the United States [4]. There are many works and methods to do in reducing greenhouse gas, CO_2 geological storage is a part of the work and a fatal method [5]. In order to achieve the Net Zero Carbon Emissions (NZCE) target by 2050, Carbon Capture, Utilization, and Storage (CCUS) is a major method (M Rashad Amir Rashidi et al., 2022) [6]. Among all of the reservoirs, gas reservoirs, depleted oil, coal seams, and saline aquifers are all good choices [1]. Bao Jia et al. [7] mentioned that CO_2 storage in unconventional reservoirs has excellent potential since the nanoporous structure could enlarge the adsorptive capacity, and organic matter has a strong affinity for CO_2. Storing CO_2 in shale formations that are producing

* Corresponding author.
E-mail address: ruichong.ni@und.edu (R. Ni).

https://doi.org/10.1016/j.heliyon.2023.e18458
Received 15 March 2023; Received in revised form 20 June 2023; Accepted 18 July 2023
Available online 20 July 2023

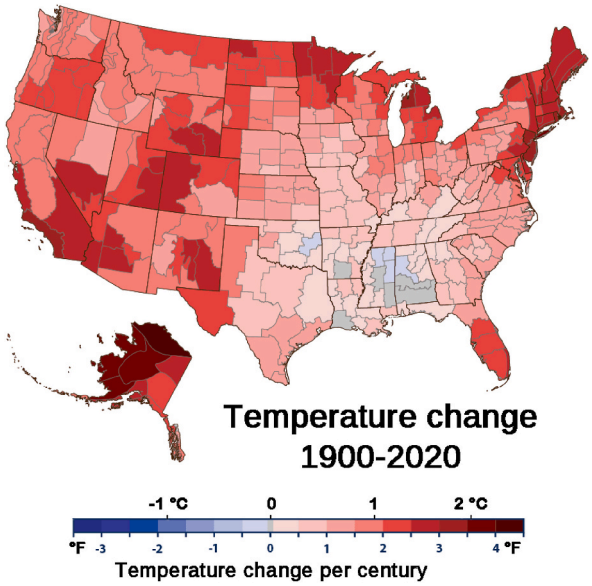

Fig. 1. Rate of temperature change in the United States, 1901–2021 [3].

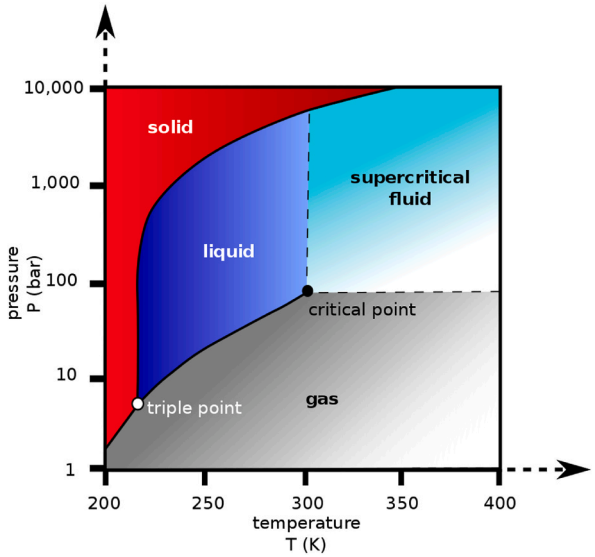

Fig. 2. Carbon dioxide pressure-temperature phase diagram [10].

unconventional gas reservoirs is also effective but receives limited attention [8].

Carbon dioxide is colorless and odorless gas at standard temperature and pressure. At this condition, the density of carbon dioxide is 1.98 kg/m^3. However, it will become a sharp, acidic odor when the concentration is high enough [9]. When the pressure and temperature are at or higher than carbon dioxide's critical temperature and critical pressure as Fig. 2 shows, it will change into an adopt properties midway between a gas and a liquid [10]. This situation is known as supercritical carbon dioxide. According to Span and Wagner [11], the CO_2 will expand to fill its container like a gas but the density is similar to liquid when it is under supercritical carbon dioxide.

The geosequestration techniques are based on knowledge and experience gained from underground natural gas storage, coal-bed methane, and oil and gas production [12]. Several researchers pointed out that hydrodynamic and geochemical processes are responsible for trapping CO_2 in target formations [13–15]. Soong et al. [16] analyzed CO_2 trapping with brine by mineral trapping. Their samples were from the Oriskany Formation, which is in Indiana County, Pennsylvania. They found that pressure and temperature are not fatal to CO_2 trapping. Kharaka et al. [17] pointed out that rapid mineral dissolution can create pathways for fluid flow in carbonate rock and cement. That will cause CO_2 and brine leak from target formations. Richa Shukla et al. [12] believed that CO_2

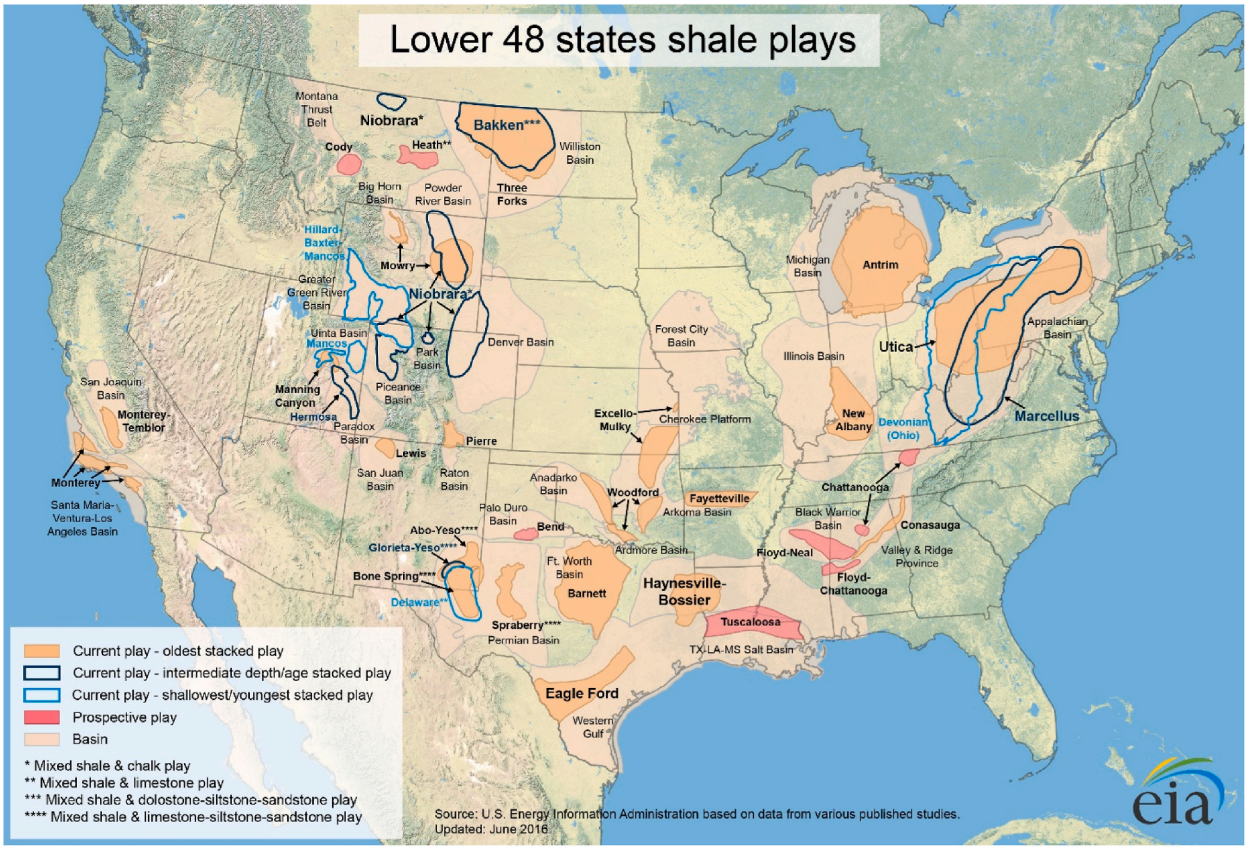

Fig. 3. Shale plays in America [18].

Table 1
Reservoir properties of shale plays.

Field	Bakken (Williston Basin)	Eagle Ford	Marcellus	Permian	New Albany
Depth (ft)	6500–10,500	4000–14000	>3000	2500–4000	1378
Porosity (%)	<10	5.2	7	4–22	10–14
Permeability (mD)	<0.1	Horizontal: 0.00111 Vertical: 0.000319	520 nD	10	150 nD
Area (square miles)	120,000 to 240,000	6130	95,000	75,000	80,000
Reservoir thickness (ft)	130	50–400	125	1300–1800	100
Reservoir pressure (psia)	0.5 to 0.78 psi/ft	5165	0.58 psi/ft	5144–5949	0.9 psi/ft
Reservoir temperature (oF)	190–220	225	140	284	86

Data collected from Refs. [19–31].

geological storage is affected by the following factors: preferential flow, CO_2 dissolution kinetics, sweep efficiency, leakage rates, mineral trapping kinetics, and the influence of stress changes on caprock and formation integrity.

Before injecting CO_2 into a reservoir, the most important question is how much gas could be stored in the reservoir. Just like buying a kettle in the supermarket, you need to estimate how much water can be filled. The different thing is, you can estimate the kettle's volume with your eyes and experience. However, you cannot see the reservoir with your eyes since it is burrowed underground. We need methods to evaluate reservoirs' CO_2 storage potential in this case.

This paper chose five methods for evaluating five shale reservoirs' CO_2 storage potential. The simplest method is to build a function between CO_2 storage capacity and the original oil in place. The second method calculates the CO_2 storage potential by gas adsorption. The third one believes both the organic material's adsorption and the shale matrix's fractures could store CO_2. The fourth method considers adsorption, residual trapping, and solubility trapping. The multiple mechanisms method takes gas adsorption, the effect of stress sensitivity, Knudson diffusion, the size of hydraulic fractures, and other factors which relate to hydraulic fractures into consideration.

Those five methods' results, advantages, and limitations are discussed in this review paper. By reading this paper, you can understand how to calculate the CO_2 storage potential for shale reservoirs. Also, this paper pointed out how to improve those methods and/or how to create a new method.

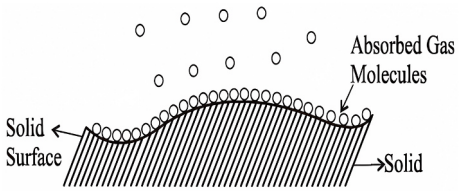

Fig. 4. Gas molecules adsorbed by solid surface [49].

2. Geologic setting of shale plays

This article chooses five shale reservoirs that have been researched for CO_2 storage in America. They are Bakken (Williston Basin), Eagle Ford, Marcellus, Permian, and New Albany shale plays. Their locations are shown in Fig. 3.

Table 1 shows the reservoir properties of those five shale plays.

The Bakken Formation is a classical unconventional tight oil play. The oil-in-place of the Bakken Formation is around several hundred billion barrels. The basin is north to southern Saskatchewan and south to northern South Dakota. The middle part of North Dakota and eastern Montana compose the basin's east and west boundary. From north to south, Williston Basin is around 475 miles long and 300 miles wide from east to west boundary. Williston basin is under the southeastern part of Saskatchewan, the southwestern part of Manitoba, the northeastern part of Montana, the east and middle part of North Dakota, and the northwestern part of South Dakota [32].

In the Middle Devonian, the Marcellus Shale was deposited in the Appalachian Basin. The collision between the Avalonian terrain and a part of the North American plate causes Acadian orogeny's movement, which is related to Marcellus shale's deposit [33,34]. Timothy R Carr et al. [35] mentioned that the Marcellus Shale is the largest shale-gas play in North America. The Marcellus shale play locates in the northeastern U.S. and across six states. Its total area is 95,000 square miles (246,000 km^2). The production zone of the Marcellus shale play is around 4000 and 6000 feet (1200–1800 m) in depth.

The Eagle Ford shale is mainly under the South-Western part of Texas state. The length of this shale play is 400 miles and the width is 50 miles [36]. There are four boundaries of Eagle Ford Play, which are the International border to Mexico in the southwest, Frio County and counties east compose the northwest boundary, Sligo Reef Margin is the southeast boundary, and the northeastern boundary is at the lower Eagle Ford [37]. The Eagle Ford overlies on the Buda limestone while overlain by the Austin chalk non-conformably [38]. Shelley et al. [39] mentioned that the productive depths of Eagle Ford range from 5000 to 18,000 ft and the thickness is from 50 to 300 ft.

The Permian basin is mainly situated in the West part of Texas and southeastern New Mexico. The Permian basin has three parts. Delaware Basin is the west part. Permian basin's center part is the Central Basin Platform. The east part is Midland Basin [17,27]. Kuuskraa et al. [17] focused on two parts of the Permian basin: The Midland and Delaware Basin. The Delaware Basin covers an area of around 10,000 square miles (25,000 km^2). Its surface elevations are ranging from roughly 3000–4500 ft (1000–1400 m) above mean sea level [40–42].

The New Albany shale is under the southeastern part of Illinois state, most counties of Indiana state, and a slim area of the northwest part of Kentucky state. According to the U.S. Department of Energy [43], the New Albany shale's area is roughly 43,500 square miles. The depth of the New Albany shale is shallow, which is from 0 to 5000 ft (0–1524 m). In southeastern Indiana, the New Albany shale's thickness is 100–140 ft (30.5–42.7 m). At the intersection of Indiana, Kentucky, and Illinois, the thickness of the Illinois Basin reaches more than 460 ft (140.2 m) [44,45].

3. Different methods for assessing CO_2 storage potential

3.1. Principles of different evaluation methods

3.1.1. A function of OOIP

Nicholas A. Azzolina et al. [46] found this method in their research. Jose A. Torres et al. [47] used this method in estimating CO_2 storage potential in Bakken. The fundamental of this method is assuming that CO_2 will replace oil during gas injection. When the CO_2 EOR method is started in the target formation, the gas is injected and oil will be produced. During this period, CO_2 will occupy the space in which oil was stored.

This method could be written in the following equation [46]:

$$CO_2\text{stored} = (\text{OOIP} \times \text{RF}) \times \text{UF}_{CO_2,\text{net}} \quad (1)$$

where: OOIP is original oil in place, STB; RF is incremental oil recovery factor, %; $UF_{CO_2,net}$ is net CO_2 utilization factor, Mscf/STB. Azzolina et al. [46] calculated net CO_2 utilization as a function of total inject volume $CO_2 + H_2O$ by multi-site empirical percentile estimates.

3.1.2. Optimized simplified local density (OSLD) model

All solid substances could attract or solute gases by solids' surface molecules when they contact with gases. This phenomenon is called "Adsorption". Adsorbent means the solids which could adsorb gases or dissolved substances. For example, the gas mask uses charcoal as an adsorbent to adsorb toxic gas to protect the wearer [48]. The adsorption could be described in Fig. 4.

Yinghui Li and Hui Pu [50] considered CO_2 adsorption amounts in shale formations based on pore size distribution. The following formula shows how they calculated the CO_2 adsorption amount:

$$\Gamma = A\int_{\sigma_{ff}/2}^{L-\sigma_{ff}/2}[\rho(z)-\rho_b(z)]dZ \tag{2}$$

where: Γ is the adsorption amount in one unit adsorbent's weight area; A is the surface area of one unit weight of the adsorbent; L is the slit width used in the model to simulate shale's pores; σ_{ff} is the molecular diameter of fluid; $\rho(z)$ is the local density at any point can be calculated; $\rho_b(z)$ is the local density of the bulk fluid.

3.1.3. Adsorbed and non-adsorbed gas

Non-adsorbed gas, which is also called "free" gas by Michael Godec et al. [25], is stored in formations' pores and fractures. The fundamental is similar to the first method. However, Michael Godec et al. [25] assume that gas is stored in all pores and fractures which not saturated by water. Similar to the previous method, effective (gas-filled) porosity could be used in calculating the volume of non-adsorbed gas in place by a volumetric approach.

Different from Yinghui Li and Hui Pu [50], Michael Godec et al. [25] calculated adsorbed gas content amount through the Langmuir adsorption model, the following equation could be used in calculating adsorbed CO_2 content:

$$V_A = (V_L \times P_R)/(P_L + P_R) \tag{3}$$

where: V_A is adsorbed gas content, scf/ton; V_L is Langmuir volume from adsorption isotherm, scf/ton; P_R is reservoir pressure, psia; P_L is average Langmuir pressure, psia.

In their theory, adsorbed CO_2 in place for each well is calculated by multiplying adsorb gas content, which could be get by the previous equation, and the tons of shale (tons per unit area). Tons of shale could be calculated by the following equation [25]:

$$\text{tons shale} = (\text{area} \times \text{thickness} \times \text{conversion factor} \times \text{shale density}) \tag{4}$$

where: tons shale is the shale mass per unit area, Mt/km^2; thickness is target area thickness, m; area is the research area's area, km^2; shale density is 2.73 t/m^3 in Marcellus Shale; conversion factor is the factor that converts t/m^3 into Mt/km^2.

For each unit volume of the reservoir, tons of shale should be computed and multiplied by adsorbed gas content. This step should be repeated for each study well. The study well's computed log curves of theoretical maximum adsorbed CO_2 could be indicated by this result. At last, sums up each study well's calculated curves, their theoretical maximum adsorbed CO_2 storage capacity could be get. Thus, the total maximum adsorbed CO_2 storage capacity of all 149 study wells could be calculated [25].

By using shale's water saturation, Michael Godec et al. [25] calculated gas-filled porosity and non-adsorbed gas in place. They also assumed that all saturated water is immobile. Thus, effective (gas-filled) porosity could be get by the following equation [25]:

$$\varphi_{effective} = \varphi_{density} \times (1 - S_w) \tag{5}$$

where: $\varphi_{effective}$ is effective (gas-filled) porosity, -; $\varphi_{density}$ is the porosity from density logs, -; S_w is the water saturation, -.

The result of each well's "free" (non-adsorbed) CO_2 storage capacity is a computed log curve. Summarizing each study well's calculated curve like calculus is the next step. In this step, we can get each well's "free" CO_2 storage capacity. Comprising "free" CO_2 storage capacity and adsorbed CO_2 storage capacity, we can get the total CO_2 storage capacity at last [25].

3.1.4. Adsorption, residual trapping, and solubility trapping

Different from the previous three simulation models, Faye Liu et al. [51] considered three CO_2 trapping mechanisms, which are gas adsorption, residual CO_2 trapping, and CO_2 solubility trapping, in their models. Faye Liu et al. [51] chose New Albany Shale as their study area. They also used numerical simulation to estimate the CO_2 storage potential.

3.1.4.1. CO_2 adsorption. The fundamental of CO_2 adsorption has discussed in chapter 3.1.2. The adsorption theory is the same as the previous method, which is Langmuir isotherm. This method calculated the extended multi-component as the following equation shows [52].

$$\omega_i = \frac{\omega_{i,max} \bullet B_i \bullet y_{ig} \bullet p}{1 + p \bullet \sum_i B_i \bullet y_{ig}} \tag{6}$$

where: ω_i is the moles of adsorbed component i per unit mass of rock, mol/ton; $\omega_{i,max}$ is the maximum moles of adsorbed component i per unit mass of rock, mol/ton; B_i is the parameter for Langmuir isotherm relation, psi^{-1}; p is the pressure, psi; y_{ig} is the molar fraction of adsorbed component i in the gas phase, – [53]. Among those parameters, B_i and $\omega_{i,max}$ are rely on lab experiments by those core samples from oil fields [30].

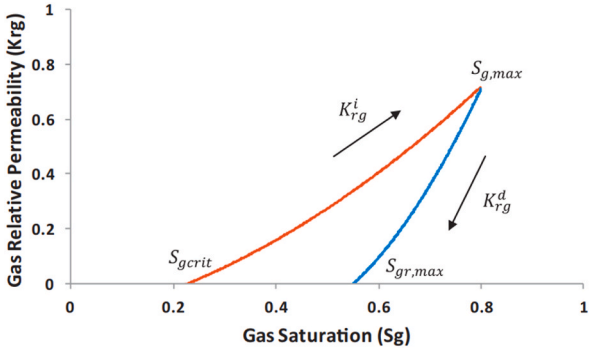

Fig. 5. S_g vs K_{rg} during gas injection and after injection (The blue line shows the drainage curve; the red line is the imbibition curve) [51]. (For interpretation of the references to color in this figure legend, the reader is referred to the Web version of this article.)

3.1.4.2. Residual CO_2 trapping and free CO_2 saturation. According to Lenormand et al. [54], the wettability and capillary effects could cause the flow dynamics of CO_2 is path-dependent when CO_2 is flowing through the water-wet reservoir. Thus, the CO_2 volume which could be drained from the reservoir is less than the CO_2 volume injected and imbibed by the reservoir. In the nonwetting phase, CO_2 will show residual entrapment. When the injection stops, the imbibition process will start. A part of nonwetting CO_2 will get disconnected and immobilized since they will become like blobs or similar to ganglia shape [55,56]. According to the theory from Land [57], Faye Liu et al. [51] assumed that the reservoir will undergo a typical drainage process and increasing gas saturation until reaches a maximum as a result. When injection stops, the imbibition process will start and causes the residually trapped gas saturation. We can calculate the residually trapped gas saturation by the following equation:

$$S_{gt} = S_{gct} + \frac{S_{g,max} - S_{gct}}{1 + C \bullet \left(S_{g,max} - S_{gct}\right)} \tag{7}$$

where: $S_{g,max}$ is the maximum gas saturation, -; S_{gt} is the residually trapped gas saturation, -; C is Land's parameter, -; S_{gct} is the critical gas saturation, -.

For your better understanding, Fig. 5 shows the meaning of those parameters in equation [7].

According to CMG [52], the following equation is for calculating the gas's relative permeability which shows in the drainage to imbibition curve in Fig. 5:

$$K^i_{rg}\left(S_g\right) = K^d_{rg}\left(S_{gf}\right) \tag{8}$$

where: K^d_{rg} is the gas relative permeability from the drainage part in Fig. 5, -; K^i_{rg} is the gas relative permeability from the imbibition part in Fig. 5, -; S_{gf} is the "free" gas saturation, -; S_g is the gas saturation, -.

The "free" gas saturation can be calculated by equation [9,52]:

$$S_{gf} = S_{gct} + \frac{1}{2}\left\{\left(S_g - S_{gr}\right) + \sqrt{\left(S_g - S_{gr}\right)^2 + \frac{4}{C}\left(S_g - S_{gr}\right)}\right\} \tag{9}$$

where: S_{gf} is the free gas saturation, -; S_{gct} is the critical gas saturation, -; S_g is the gas saturation, -; S_{gr} is the residual gas saturation, -.

3.1.4.3. Solubility trapping. Carbon dioxide is soluble in water. According to Stumm and Morgan [58], Henry's law could give us instruction in calculating reservoir fluid's solubility of injected CO_2. Henry's law could be written by the following equation:

$$x_{CO_2} = \frac{f_{CO_2}}{H_{CO_2}} \tag{10}$$

where: x_{CO_2} is the mole fraction of CO_2 dissolved in brine, -; f_{CO_2} is the CO_2 fugacity, psi; H_{CO_2} is CO_2 Henry's law constant, psi. f_{CO_2} is a factor that could be get by Peng and Robinson's equation of state.

H_{CO_2} is calculated by equation [11]. In equation [11], $H^*_{CO_2}$ and $V^\infty_{CO_2}$ can be get by the method found by Li and Nghiem's [59]:

$$H_{CO_2} = H^*_{CO_2} \bullet \exp\left[V^\infty_{CO_2} \bullet \frac{p - p_{ref}}{RT}\right] \tag{11}$$

where: $H^*_{CO_2}$ is Henry's law constant under the reference pressure, psi; p_{ref} is the reference pressure, psi; $V^\infty_{CO_2}$ is the partial molar volume of CO_2 when the CO_2 is in infinite dilution, mol; p is the pressure, psi; T is the thermodynamic temperature, K; R is the gas constant, which is equal to 0.082057 $L{\cdot}atm{\cdot}K^{-1}{\cdot}mol^{-1}$.

At the same time, Faye Liu et al. [51] pointed out that gas solubility will decrease with salinity increases and this is called the

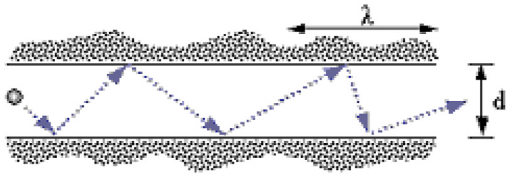

Fig. 6. Knudsen diffusion in a cylindrical pore [62].

"salting-out effect". This phenomenon was also taken into consideration in their model and it could be calculated by using the method from Bakker [60]:

$$\ln\left(\frac{H_{salt,CO_2}}{H_{CO_2}}\right) = k_{salt,CO_2} \bullet m_{salt} \tag{12}$$

where: H_{salt,CO_2} is Henry's constant of CO_2 which is solute in brine, psi; H_{CO_2} is Henry's constant of CO_2 which is solute in distilled water, psi; m_{salt} is the salt's molality which is dissolved in pure water, mol/kg; k_{salt,CO_2} is the CO_2 salting-out coefficient, kg/mol.

3.1.5. Multiple mechanisms

Chen Zhiming et al. [61] published a method to evaluate New Albany Shale's CO_2 storage capacity that takes gas adsorption, the effect of stress-sensitivity, Knudson diffusion, the size of hydraulic fractures, and other factors which relate to hydraulic fractures into consideration.

When particles are involved in a system, take shale's pore, for example, they will have a free path. If the pore's scale length is smaller or similar to the particles' free path, Knudson diffusion occurs. Particles will collide with the pores' wall many times if particles flow into long and narrow pores (2–50 nm) and Knudson diffusion occurs. Fig. 6 shows the case of Knudson diffusion [62]. When CO_2 flows into shale matrix from natural fractures, the Knudson diffusion could be used in calculating the flow speed as a factor.

The gas adsorption is already discussed in chapter 3.1.2. It means the shale matrix's ability in adsorbing CO_2.

Rock's petrophysical parameters will change if the effective stress is alternating. Rock stress sensitivity shows how much they will change. Those parameters include porosity, permeability, and electrical resistivity [63]. In their method, only the effect of stress sensitivity related to sensitivity between reservoir permeability and pressure was taken into consideration. Both reservoir pressure and shale permeability will increase when CO_2 is injected. This increase has a positive effect on CO_2 storage.

As for hydraulic fractures, Chen Zhiming et al. [61] believed that the fracture length is larger than the fracture width and CO_2 mainly flows in formations from fracture faces. Thus, they assumed that hydraulic fractures' tips are sealed boundaries. To build the mass conservation equation and figure out how much the gas flow rate in fractures is, they built a dimensionless mathematical model in their study based on Pedrosa's substation [64]. Mukherjee and Economides [65] found a method that considered the wellbore storage effect and skin factor due to hydraulic fractures. This method is also used in the article from Chen Zhiming et al. [61].

The estimated CO_2 storage capacity is shown in equation [13].

$$Q_D = 4 n_F T_D \tag{13}$$

where: Q_D is total CO_2 injection volume, m^3; n_F is hydraulic fracture number, -; T_D is total injection time, days; q_{inD} is injection rate, 10^5 m^3/d [61].

In this equation, the total injection time T_D is a function of Knudson diffusion, adsorption index, stress-sensitivity coefficient, and hydraulic fractures' size.

3.2. Different ways to use CO_2 storage potential evaluation methods

3.2.1. A function of OOIP

3.2.1.1. Calculate directly. According to Jose A. Torres et al. [47], the OOIP in Bakken ranges from 300 billion to 900 billion barrels. The estimated incremental oil recovery range of 0.6%–5.4%. The net CO_2 utilization is 1.8 Mscf per barrel. CO_2 in Bakken formations is 19.25 Mscf per t under reservoir conditions, which is the same as Nicholas A. Azzolina et al. [46]. They believed that CO_2 storage volume ranged from 169 Mt to 1.5 Gt in Bakken.

3.2.1.2. Cyclic CO_2 injection with numerical simulation. Kuuskraa et al. [24] calculated CO_2 storage potential in their study area by using numerical simulation. In chapter 3.1.1, we have already discussed the mechanism of CO_2 storage potential which is used in this numerical simulation model. Their steps are to build a simulation model and validated the model by history matching. At last, provide recovery estimates and CO_2 storage volume during the CO_2 injection. Four shale oil reservoirs in America were selected by them, which are Midland Basin's Wolfcamp Shale, Delaware Basin, Williston Basin Bakken Shale, and Lower Eagle Ford Shale.

Cyclic CO_2 injection was used in their model. The injection was assumed to start after five years and 272,000 barrels of primary production. 17 MMcfd CO_2 was injected in two months at the first cycle. The bottom hole pressure was limited to 4800 psia. After the

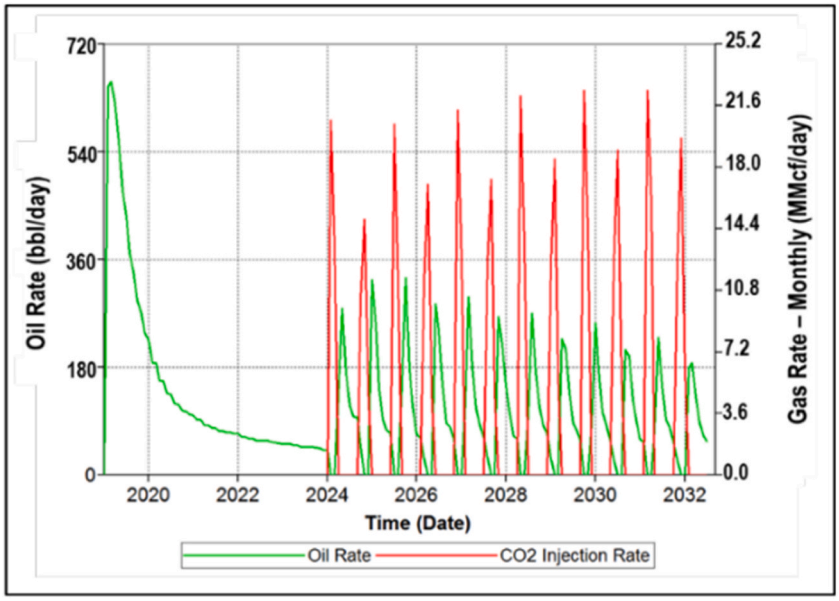

Fig. 7. Cyclic CO_2 injection rate in simulation model [24].

Table 2
CO_2 Storage from CO_2 Cyclic injection EOR: Four Shale Oil Basins [24].

Shale Basin/Formation	Storage of CO_2, Gt
Williston Basin/Bakken Shale	2.3
South Texas/Eagle Ford Shale	2.9
Midland Basin/Wolfcamp Shale	9.8
Delaware Basin/Wolfcamp Shale	15.1

Table 3
Parameters of OSLD model [50].

Parameters	Value
Reservoir permeability, μD	1
Reservoir temperature, °F	240
Initial reservoir pressure, psi	3200
Porosity, %	20
Initial water saturation, %	10
Inject time, days	100
Inject amount, pore volume, PV	0.57

injection, 2 weeks of soaking and 6 months of production followed. As Fig. 7 shows, there were 12 cycles were simulated in their model.

By processing cyclic CO_2 injection, 9.8 Gmt of CO_2 would be stored in Midland Basin. They also simulated the CO_2 storage amount in other different basins by cyclic CO_2 injection as Table 2 shows.

We can see that the CO_2 storage amount from Kuuskraa et al. [24] is not the same as Jose A. Torres et al. [47], not even close. The reason is reservoir properties used by Jose A. Torres et al. [47] are different from those by Kuuskraa et al. [24]. For example, Jose A. Torres et al. [47] believed that the OOIP in Bakken ranges from 300 billion to 900 billion barrels while Kuuskraa et al. [24] used 90.8 billion barrels in their model.

3.2.2. Optimized simplified local density (OSLD) model

Yinghui Li and Hui Pu [50] built a 1-D model in their paper and the size is 6.25 ft × 0.25 ft × 0.5 ft, which are length, width, and thickness. Those parameters used in their model are shown in Table 3.

According to their simulation model's result, the total CO_2 storage amount is 0.36 PV, which is equal to 0.05625 ft^3 (0.0016 m^3).

Table 4
The total maximum CO_2 storage capacity in the study area [25].

	New York	Pennsylvania	West Virginia	Eastern Ohio & West Virginia Panhandle	Total
Potential CO_2 storage area, km^2	14,151	49,472	34,167	9108	106,898
Adsorbed gas in place, km^3	1.485×10^{21}	9.838×10^{21}	3.663×10^{21}	0.949×10^{21}	15.935×10^{21}
Non-adsorbed, 'free', gas in-place, km^3	1.447×10^{21}	14.07×10^{21}	4.16×10^{21}	1.184×10^{21}	20.861×10^{21}
Total gas in-place, km^3	2.931×10^{21}	23.908×10^{21}	7.823×10^{21}	2.133×10^{21}	36.796×10^{21}
Maximum CO_2 storage, adsorbed, t	1.0926×10^{10}	5.9083×10^{10}	2.2434×10^{10}	0.629×10^{10}	98.733×10^{10}
Maximum CO_2 storage, 'free', t	0.6268×10^{10}	4.4455×10^{10}	1.6548×10^{10}	0.5226×10^{10}	72.496×10^{10}
Total CO_2 storage capacity, t	1.7194×10^{10}	10.3538×10^{10}	3.8982×10^{10}	1.1516×10^{10}	171.229×10^{10}
Total maximum CO_2 storage capacity per unit area, t/km^2	1,220,000	2,090,000	1,140,000	1,260,000	1,600,000

Table 5
Reservoir parameters [66].

Parameters	Value
Reservoir permeability, μD	0.63
Pemieability fracture, μD	2
Langmuir adsorption CO_2, 1/psi	0.004
Langmuir adsorption Fracture CO_2, 1/psi	0.002
Depth, ft	6508
Porosity, %	9.71
Porosity fracture, %	0.1
Fracture stages, –	21
Fracture width, ft	0.001
Fracture half length, ft	350

Table 6
CO_2 sequestration amount under different injection pattern, ft^3 [66].

Inject type	Continuous injection	Cyclic injection
Inject pressure, psi		
2000	8.64×10^9	–
3000	1.78×10^{10}	1.40×10^{10}

3.2.3. Adsorbed and non-adsorbed gas

As we discussed in chapter 3.1.3, this method calculates the CO_2 storage potential by adding adsorbed gas and non-adsorbed gas. All data were got from well logging and adsorption isotherm data.

According to Michael Godec et al. [25], the maximum CO_2 storage capacity of each part of Marcellus Shale is shown in Table 4.

Qin He et al. [66] also chose Marcellus Shale play as their study area. Their basic theory is the same as Michael Godec et al. [25] and their parameters for simulation model are shown in Table 5.

Different from Michael Godec et al. [25], Qin He et al. [66] tried two inject type and two inject pressure, which are continuous injection and cyclic injection, 2000 psi and 3000 psi. The total amount of CO_2 storage is shown in Table 6.

3.2.4. Adsorption, residual trapping, and solubility trapping

This model is based on the New Albany Shale. Faye Liu et al. [51] only focused on a 62-acre (250,905 m^2) with two hydraulic fracture networks since the software will cost too much time in simulating if the study area is 326 acres. Table 7 shows reservoir properties inputted in their simulation model.

Faye Liu et al. [51] performed three simulated cases of CO_2 injection and storage as Table 8 shows. In the first case, it only considered CO_2 injection, without hysteresis and CO_2 solubility. The second case considered both CO_2 injection and hysteresis, but without CO_2 solubility. The third case calculated all three CO_2 trapping mechanisms, which are CO_2 injection, hysteresis, and CO_2 solubility. However, the third case was built in 2-D, which is different from the previous two cases. The first and second cases are calculated in 3-D. Their model has to solve those involved chemical reaction equations simultaneously. As a result, computational demand must be added. This is why the third case was built-in 2-D, to speed up the calculation process.

3.2.5. Multiple mechanisms

Chen Zhiming et al. [61] also chose New Albany Shale to verify their theory. The geological setting of New Albany Shale has been

Table 7
Reservoir and wells' parameters used in the simulation [51].

	Properties	Values
Reservoir properties	Temperature, ℃	30 (86 °F)
	Thickness, m	30 m (100 ft)
	Depth, m	420 m (1378 ft)
	Initial pressure gradient, kPa/m	6.8 (0.3 psi/ft)
	Porosity, %	10–14
	Pressure gradient, kPa/m	20.4 (0.9 psi/ft)
	Diffusivity, m^2/s	1×10^{-9}
	Permeability, nD	150
	Rock density, g/cm^3	2.4
	Water saturation, %	40
	Natural fracture conductivity, μD-m	6 (20 μD-ft)
Rock geochemistry properties	Total organic content (TOC), %	12
	Maximal adsorbed gas (CO_2), m^3/ton	14.4 (510.1 scf/ton)
	Langmuir adsorption constant (CO_2), psi^{-1}	0.000896
Rock geomechanical properties	Matrix compressibility, Pa^{-1}	4.35×10^{-10} (3×10^{-6} psi^{-1})
	Fracture compressibility, Pa^{-1}	4.35×10^{-8} (3×10^{-4} psi^{-1})
Well properties	Well length, m	1280 (4200 ft)
	CO_2 injection rate, m^3/day	2832 (100,000 MMscf/day)
	Fracture stages, -	4
	Fracture conductivity, mD-m	30 (100 mD-ft)
	Fracture half-length, m	137 (450 ft)
	Fracture width, m	0.61 (2 ft)

Table 8
Simulation Result [51].

	First Case	Second Case	Third Case
Adsorption Gas Amount, m^3	4.98×10^6	4.89×10^6	4.90×10^6
Free Gas Amount, m^3	0.2075×10^6	0.22×10^6	2.28×10^5
Residual Gas Amount, m^3		1.13×10^4	1.84×10^4
Dissolved Gas Amount, m^3			5.66×10^4

Table 9
CO_2, well, rock, and reservoir's average parameters in the study area [61].

Items	Properties	Value
Rock	Matrix compressibility, MPa^{-1}	4.4×10^{-4}
	Knudsen diffuse coefficient, -	0.0162
	Natural fracture compressibility, MPa^{-1}	0.042
	Porosity, %	12
	Matrix permeability, D	1.5×10^{-7}
	Density, ton/m^3	2.4
	Natural fracture permeability, D	0.001
Reservoir	Depth, m	420
	Depleted pressure, MPa	0.6
	Temperature, K	303.15
	Control area, m^2	7.07×10^6
	Thickness, m	30
Well	Hydraulic fracture stages, –	4
	Well length, m	1280
	The storage coefficient of wellbores, -	1
	Constrained pressure, MPa	7.2
	The injection rate of CO_2, m^3/d	1×10^5
	Hydraulic fractures' half-length, m	137
	Fracture number, –	4
	Skin factor, –	0.1
CO_2	Viscosity, mPa·s	0.01
	Adsorption index, –	4.8
	Maximal adsorbed gas, m^3/ton	13.8
	Compressibility, MPa^{-1}	0.048
	Z-factor, –	0.8

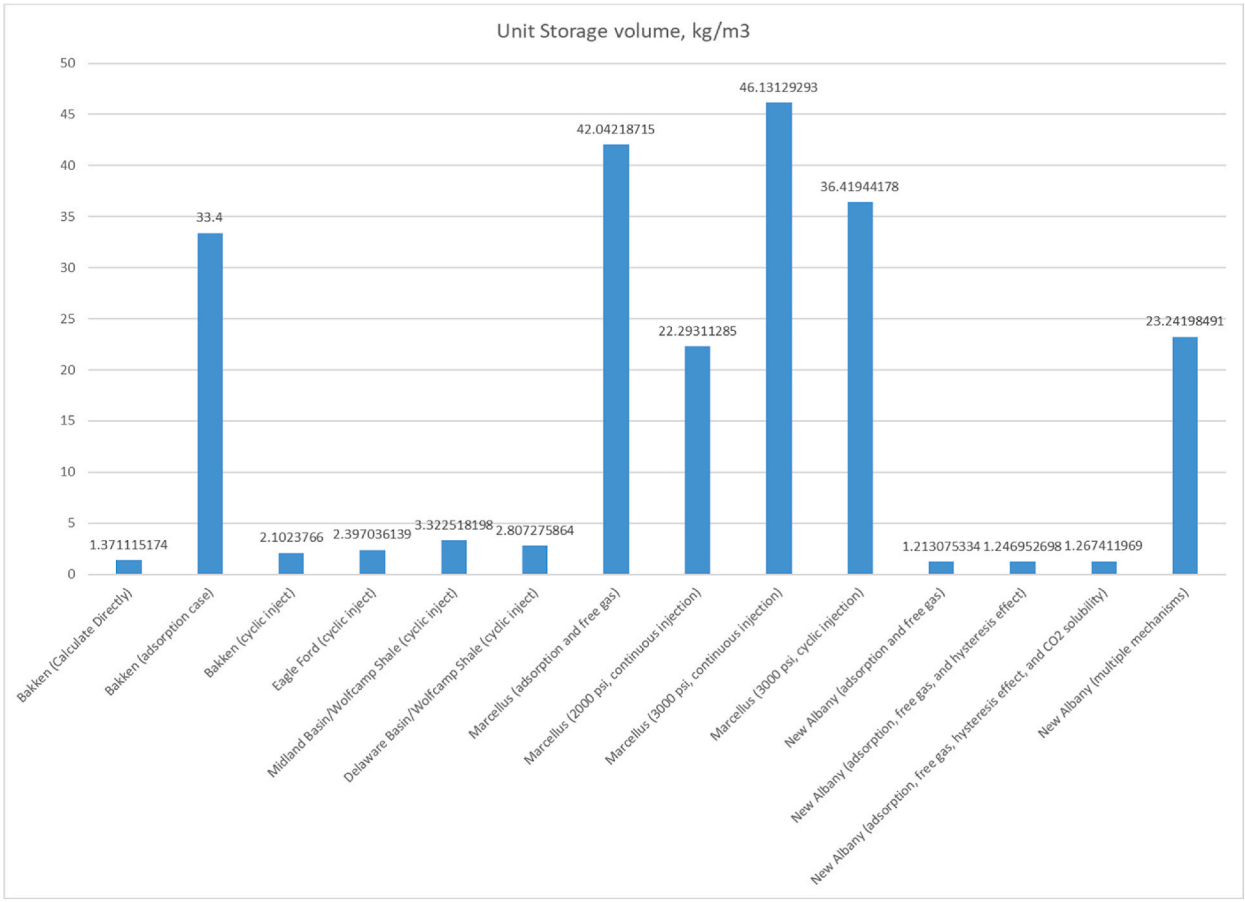

Fig. 8. Unit storage capacity of each shale reservoir.

discussed in chapter 2. Table 9 listed those parameters which are necessary for the simulation.

Chen Zhiming et al. [61] assumed the whole study area is homogenous and the reservoir is already depleted. During the injection and storage, they supposed that the CO_2 is kept gas phase. The reason is that the New Albany Shale is relatively shallow and the target formations' lithostatic pressure is around 8.55 MPa. If they used liquid-phase CO_2, the wellbore pressure will be higher than the lithostatic pressure and causes geological damage. The CO_2 injection they used is 7.2 MPa.

4. Discussion

This article calculated unit storage capacity, which is how much gas can be stored in one cubic meter, for all five methods. Fig. 8 shows the unit storage capacity.

By reading this figure, we can see that the Marcellus shale play used the "adsorbed and non-adsorbed gas" method, continuous inject pattern and 3000 psi inject pressure shows the most optimistic result. We can say that the Marcellus shale play is more suitable than other shale plays. At least, Marcellus shale play is better than New Albany. We can also compare the result between continuous injection and cyclic injection under 3000 inject pressure. It shows that continuous injection pattern could store two times amount of CO_2 than cyclic injection pattern. Let us see the result of New Albany which also used the "adsorbed and non-adsorbed gas" method in the simulation. Its unit storage volume is far less than that in Marcellus.

Comparing those three cases in Bakken shale, the unit storage capacity calculated by the OSLD model is over ten times larger than the other two cases. Among those three cases, only the OSLD considered pore size distribution. Compared with the cyclic inject case, the OSLD model did not use the Langmuir adsorption model but the cyclic inject case was used. In my opinion, this is why the OSLD model's result is different from the cyclic inject case. According to Masel and Richard (1996) [67], the Langmuir adsorption model has the following assumptions:

i. The adsorbing sites' surface is perfectly flat plane and homogeneous.
ii. The adsorbing gas is adsorbed into immobile state.
iii. All sites are energetically equivalent and equally adsorb the energy.

Table 10
Parameters used in New Albany simulation models [51,61].

Methods Parameters	Adsorption, residual trapping, and solubility trapping	Multiple mechanisms
Reservoir properties		
Depth, m	420	420
Thickness, m	30	30
Temperature, °C	30	30
Porosity, %	10–14	12
Matrix permeability, nD	150	150
Rock density, g/cm^3	2.4	2.4
Rock geomechanical properties		
Matrix compressibility, MPa^{-1}	4.35×10^{-4}	4.4×10^{-4}
Fracture compressibility, MPa^{-1}	4.35×10^{-2}	4.2×10^{-2}
Well properties		
Well length, m	1280	1280
Fracture stages, –	4	4
Fracture half-length, m	137	137
CO_2 inject rate, m^3/day	2832	100,000

iv. Each site has can hold one or more molecules.
v. No (or ideal) interactions between adsorbate molecules and their adjacent sites.

For the first assumption, the pores' surface of shale cannot be perfectly flat and homogeneous. Also, the pores' surface cannot be immobile. Sai Wang et al. (2019) [68] mentioned that carbonic acid will react with shale's minerals. Their experiments result also pointed out that the pore size distribution will change after CO_2 submerge. Thus, the OSLD model can do better in simulating the real situation during CO_2 injection and storage than the Langmuir adsorption model. Furthermore, building a model which takes how will pore size distribution changes during CO_2 injection and storage could be a good choice.

Let us compare these four cases of New Albany. The results of the "adsorption and free gas" method, "adsorption, free gas, and hysteresis effect" method, and "adsorption, free gas, hysteresis effect, and dissolved gas" method are similar to each other, which is more than 1.2 kg/m^3. However, the "multiple mechanisms" method's simulation result is 23.24 kg/m^3. Why their results are so different? The reason could be complex. The following Table 10 shows their parameters.

We can see in Table 10, those parameters used by the two methods are almost the same, except for the CO_2 inject rate. Besides, the "adsorption, residual trapping, and solubility trapping" method assumed that water saturation is still 40% but the "multiple mechanisms" method does not take consider the formation water.

In my opinion, there might be three reasons that could cause their results different:

i. The CO_2 inject rate is fatal to the unit storage volume since the more optimistic one injects CO_2 35 times quicker than the other one.
ii. The Knudsen diffusion plays an important role in CO_2 storage. If we can deplete water in the reservoir and let Knudsen diffusion happens more frequently, the CO_2 storage volume could increase many times.
iii. Chen Zhiming et al. [61] considered the skin factor but Faye Liu et al. [51] did not. Formation damage and near-well vicinity situation could also affect CO_2 storage potential.

In fact, the Knudsen diffusion is an important factor that could affect gas permeability in shale. Thus, the method from Chen Zhiming et al. [61] has only one more factor than the method from Michael Godec et al. [25], which is stress-sensitivity.

Almost all of nowadays simulation models for calculating CO_2 storage potential focus on reservoir properties, but nearly nobody considered well integrity. Those five methods discussed in this paper supposed that all CO_2 will stay in the target formation during gas injection. However, CO_2 will leak from the subsurface to the surface through different pathways [1,69,70]. Mingxing Bai et al. [1] believed that the vertical permeability of cement plays the most critical role. Ana Widyanita and W Ahmad Rafael B W Zairudin [70] also mentioned that long-term reaction between carbonic acid and cement will increase the cement's permeability. Thus, assuming no gas is leaking, which is used by those methods in this paper, is not realistic.

5. Conclusions

i. Marcellus shale play is the most suitable place in CO_2 storage among the five shale plays discussed in this paper.
ii. CO_2 inject rate could affect formations' storage potential. The higher the CO_2 injection rate, the more CO_2 can be stored in the reservoir.
iii. Knudsen diffusion happens in dry pores while CO_2 solubility trapping needs water. As we know that the water saturation can be neither 0% nor 100%. Taking adsorption, residual trapping, solubility trapping, and Knudsen diffusion into consideration is a more realistic way to evaluate CO_2 storage potential.

Recommendations

i. Knudsen diffusion is one of the important factors in CO_2 storage. However, it is not the only transport mechanism of CO_2. If we can base on pore size distribution data and add more transport mechanisms for those pores larger than 50 nm, the result would be more accurate.
ii. During CO_2 injection and storage, formations' pore size distribution, and thus, relative permeability will also change. If we can figure out how the pore size distribution could change and bring the variation trend into the simulation, the simulation result could be more accurate than before.
iii. Most researchers focused on numerical simulation but few of them proved their results in lab experiments or an oil field. If we can process some experiments in the lab or choose one well to see how much CO_2 could be stored, that will be more convictive.
iv. Not all of the oil fields will choose CO_2 injection as the first EOR method. It could be a valuable topic to simulate CO_2 storage potential in those oil fields which processed other EOR methods like polymer, alkali, surfactant, and so on.
v. Few researchers have studied formations' geomechanical properties. How those properties will change during CO_2 injection and storage could be a fruitful topic for our researchers.

iv. Taking well integrity, especially cement quality, and permeability into the simulate model would be tallying with the real situation in shale fields.
v. Shale's geomechanical properties, such as permeability, young's modulus, and Poisson's ratio, could also be fatal to CO_2 injection.

Author contribution statement

All authors listed have significantly contributed to the development and the writing of this article. </p>

Data availability statement

Data included in article/supp. material/referenced in article.

Declaration of competing interest

The authors declare that they have no known competing financial interests or personal relationships that could have appeared to influence the work reported in this paper.

Acknowledgment

The author wants to say thank you to Dr. Ling for his patience and great guidance in this work. Special thanks to the University of North Dakota (UND) for its financial support.

Nomenclature

area research area's area, km^2
B_i parameter for Langmuir isotherm relation, psi^{-1}
C Land's parameter, –
conversion factor the factor that converts mass per unit volume into mass per unit area
f_{CO_2} CO_2 fugacity, psi
H_{CO_2} Henry's law constant for CO_2, psi (in equation [3.10]); Henry's constant of CO_2 which is solute in pure water, psi (in equation [3.12])
$H^*_{CO_2}$ Henry's law constant of CO_2 at the reference pressure, psi
H_{salt,CO_2} Henry's constant of CO_2 which is solute in brine, psi
K^d_{rg} gas relative permeability from the drainage part, –
K^i_{rg} gas relative permeability from the imbibition part, –
k_{salt,CO_2} CO_2 salting-out coefficient, kg/mol
m_{salt} salt's molality which is dissolved in pure water, mol/kg

n_F hydraulic fracture number, –
OOIP original oil in place, STB
p pressure, psi
P_L average Langmuir pressure from adsorption isotherm data, psia
p_{ref} reference pressure, psi
P_R reservoir pressure, psia
Q_D total CO_2 injection volume, m^3
q_{inD} injection rate, 10^5 m^3/d
R gas constant, 0.082057 $L{\cdot}atm{\cdot}K^{-1}{\cdot}mol^{-1}$
RF incremental oil recovery factor, %
shale density 2.73 g/cc in Marcellus Shale
S_g gas saturation, –
S_{gct} critical gas saturation, –
S_{gf} free gas saturation, –
$S_{g,max}$ maximum gas saturation, –
S_{gr} residual gas saturation, –
S_{gt} residually trapped gas saturation, –
S_w water saturation, –
T temperature, K
T_D total injection time, days
thickness target area thickness, ft
Tons shale shale mass per unit area, Mt/km^2
$UF_{CO_2,net}$ net CO_2 utilization factor, Mscf/STB
V_A adsorbed gas content, scf/ton
$V^{\infty}_{CO_2}$ partial molar volume of CO_2 when the CO_2 is in infinite dilution, mol
V_L Langmuir volume from adsorption isotherm, scf/ton
x_{CO_2} mole fraction of CO_2 dissolved in the aqueous phase, –
y_{ig} the molar fraction of adsorbed component i in the gas phase, –
$\varphi_{density}$ porosity from density logs, –
$\varphi_{effective}$ effective (gas-filled) porosity, –
ω_i moles of adsorbed component i per unit mass or rock, mol/ton
$\omega_{i,max}$ maximum moles of adsorbed component i per unit mass of rock, mol/ton

References

[1] Mingxing Bai, Kaoping Song, Li Yang, Jianpeng Sun, Kurt M. Reinicke, Development of a novel method to evaluate well integrity during CO_2 underground storage, SPE J. 20 (2015) 628–641.
[2] Earth day: U.S. Warming rankings, in: Climate Central, 2023. https://www.climatecentral.org/climate-matters/earth-day-warming-rankings.
[3] Climate change indicators: U.S. And global temperature, in: EPA.gov. Environmental Protection Agency, 2023. https://www.epa.gov/climate-indicators/climate-change-indicators-us-and-global-temperature.
[4] Inventory of U.S. Greenhouse gas emissions and sinks, in: EPA.gov. Environmental Protection Agency, 2023 Jan 12. https://www.epa.gov/ghgemissions/inventory-us-greenhouse-gas-emissions-and-sinks.
[5] A. Iogna, J. Guillet-Lhermite, C. Wood, Perenco, and J. P. Deflandre, CO_2 Storage and Enhanced Gas Recovery: Using Extended Black Oil Modelling to Simulate CO_2 Injection on a North Sea Depleted Gas Field, 79th EAGE Conference and Exhibition June 12–15, 2017, (Paris, France).
[6] M. Rashad Amir Rashidi, , Edgar Peter Dabbi Ahmad Ismail Azahree, Zainol Affendi Abu Bakar, Dylon Tan Jen Huang, Claus Pedersen, Pankaj K. Tiwari, M. Taufik, M. Sallehud-Din, M. Azim Shamsudin, M. Khaidhir Hamid, Tewari Raj, Parimal A. Patil, CO_2 leakage marine dispersion modelling for an offshore depleted gas field for CO_2 storage, in: Offshore Technology Conference Asia March 22 - 25, Kuala Lumpur, Malaysia, 2022.
[7] Bao Jia, Zeliang Chen, Chenggang Xian, Investigations of CO_2 storage capacity and flow behavior in shale formation, J. Petrol. Sci. Eng. 208 (2022), https://doi.org/10.1016/j.petrol.2021.109659. ISSN 0920-4105.
[8] Gray, Kimberly. Carbon Sequestration Atlas of the United States and Canada (Third Edition). United States. https://doi.org/10.2172/1814019.
[9] Carbon dioxide, in: Wikipedia, 2023. https://en.wikipedia.org/wiki/Carbon_dioxide.
[10] Supercritical carbon dioxide, in: Wikipedia, 2023. https://en.wikipedia.org/wiki/Supercritical_carbon_dioxide.
[11] Roland Span, Wolfgang Wagner, A new equation of state for carbon dioxide covering the fluid region from the triple-point temperature to 1100 K at pressures up to 800 MPa, J. Phys. Chem. Ref. Data 25 (6) (1996) 1509–1596.
[12] Richa Shukla, Pathegama Ranjith, Asadul Haque, Xavier Choi, A review of studies on CO2 sequestration and caprock integrity, Fuel 89 (10) (2010) 2651–2664.
[13] S. Bachu, J.J. Adams, Sequestration of CO_2 in geological media in response to climate change: capacity of deep saline aquifers to sequester CO_2 in solution, Energy Convers Mgmt 44 (20) (2003) 3151–3175.
[14] W.D. Gunter, S. Bachu, S. Benson, Spl Pub 233, The Role of Hydro-Geological and Geochemical Trapping in Sedimentary Basins for Secure Geological Storage of Carbon Dioxide, Geological Society, London, 2004, pp. 129–145.
[15] T. Xu, J.A. Apps, K. Pruess, Mineral sequestration of carbon dioxide in a sandstone-shale system, Chem. Geol. 217 (2005) 295–318.
[16] Y. Soong, A.L. Goodman, J. R McCarthy-Jones, J. P Baltrus, Experimental and simulation studies on mineral trapping of CO_2 with brine, Energy Convers. Manag. 45 (2004) 1845–1859.
[17] Y.K. Kharaka, D.R. Cole, S.D. Hovorka, W.D. Gunter, K.G. Knauss, B.M. Freifeld, Gas–water–rock interactions in Frio Formation following CO_2 injection: implications for the storage of greenhouse gases in sedimentary basins, Geology 34 (7) (2006) 577–580.
[18] Lower 48 states shale plays, in: U.S. Energy Information Administration, 2023. https://www.eia.gov/maps/maps.htm.

[19] Three forks formations, Williston Basin, North Dakota and Montana (USGS). https://wiki.aapg.org/Bakken, 2023.
[20] Bakken Formation, in: Wikipedia, 2023. https://en.wikipedia.org/wiki/Bakken_Formation.
[21] Ling, Kegang , Shen, Zheng , Han, Guoqing , He, Jun, and Pei Peng, A Review of Enhanced Oil Recovery Methods Applied in Williston Basin, Unconventional Resources Technology Conference August 25-27, 2014, Denver, Colorado. doi: https://doi.org/10.15530/URTEC-2014-1891560.
[22] Eagle ford shale, in: Geology.com, 2023. https://geology.com/articles/eagle-ford.
[23] Ian Lopez, Khaled Enab, and Youssef Elmasry, Improving CO2 Storage and Oil Recovery in Shale Oil Reservoirs Using Dual Lateral Wells, Unconventional Resources Technology Conference June 20-22 2022, Houston, Texas, USA.
[24] Kuuskraa, V., Oudinot, A. Y., Petrusak, R., & Murray, B, An Emerging CO_2 Storage Option: CO_2 Storage and By-Product Oil Recovery from Shale Oil Formations, 15th Greenhouse Gas Control Technologies Conference March 15-18, 2021, Abu Dhabi, UAE.
[25] Michael Godec, Koperna George, Robin Petrusak, Anne Oudinot, Assessment of factors influencing CO_2 storage capacity and injectivity in eastern U.S. Gas shales, Energy Proc. 37 (2013) 6644–6655, https://doi.org/10.1016/j.egypro.2013.06.597.
[26] Marcellus shale, in: American Petroleum Institude, 2023. https://www.api.org/oil-and-natural-gas/energy-primers/hydraulic-fracturing/marcellus-shale.
[27] EIA, Permian Basin Part 2 Wolfcamp Shale Play of the Midland Basin Geology Review, Department of Energy, Energy Information Administration, 2020. https://www.eia.gov/maps/pdf/Permian_Wolfcamp_Midland_EIA_reportII.pdf.
[28] EIA, Permian Basin Wolfcamp Shale Play Geology Review, U.S. Department of Energy, Energy Information Administration, 2018. https://www.eia.gov/maps/pdf/PermianBasin_Wolfcamp_EIAReport_Oct2018.pdf.
[29] Jean-Philippe Nicot, Roxana Darvari, Peter Eichhubl, Bridget R. Scanlon, A. Brent, L. Elliott, Taras Bryndzia, F.W. Julia, Gale, András Fall, Origin of low salinity, high volume produced waters in the Wolfcamp Shale (Permian), Delaware Basin, USA, Applied Geochemistry 122 (2020), https://doi.org/10.1016/j.apgeochem.2020.104771. ISSN 0883-2927.
[30] D. Strapoc, M. Mastalerz, A. Schimmelmann, A. Drobniak, N.R. Hasenmueller, Geochemical constraints on the origin and volume of gas in the new Albany shale (Devonian–Mississippian), eastern Illinois basin, AAPG Bull. 94 (11) (2010) 1713–1740.
[31] Terence Hamilton-Smith, Gas Exploration in the Devonian Shales of Kentucky, Bulletin 5 (1993). https://uknowledge.uky.edu/kgs_b/5.
[32] T.J. Heck, R.D. LeFever, D.W. Fischer, J. LeFever, Overview of the Petroleum Geology of the North Dakota Williston Basin, North Dakota Geological Survey, Bismarck, ND, 2002.
[33] H. Williams, R.D. Hatcher Jr., Suspect terranes and accretionary history of the Appalachian orogen, Geology 10 (10) (1982) 530–536.
[34] F.R. Ettensohn, Controls on the origin of the devonian-mississippian oil and gas shales, east-Central United States, Fuel 71 (12) (1992) 1487–1492, https://doi.org/10.1016/0016-2361(92)90223-B.
[35] Timothy R. Carr, Guochang Wang, McClain Taylor, Petrophysical analysis and sequence stratigraphy of the utica shale and Marcellus shale, in: Appalachian Basin, USA, International Petroleum Technology Conference March 26–28, 2013 (Beijing, China).
[36] Gong, X., Tian, Y., McVay, D. A., Ayers, W. B., & Lee, J., Assessment of Eagle Ford Shale Oil and Gas Resources, SPE Unconventional Resources Conference-Canada November 5–7, 2013, Calgary, Alberta, Canada. doi: https://doi.org/10.2118/167241-MS.
[37] T.F. Hentz, W.A. Ambrose, D.C. Smith, Eaglebine play of the southwestern east Texas basin: stratigraphic and depositional framework of the upper cretaceous (Cenomanian-Turonian) woodbine and eagle ford groups, AAPG (Am. Assoc. Pet. Geol.) Bull. 98 (12) (2014) 2551–2580, https://doi.org/10.1306/07071413232.
[38] Nwabuoku, K. C, Increasing lateral coverage in eagle ford horizontal shale completion, SPE Annual Technical Conference and Exhibition October 30–November 2, 2011, Denver, Colorado, USA. https://doi.org/10.2118/147549-MS.
[39] Shelley, R., Saugier, L., Al-Tailji, W., Guliyev, N., & Shah, K., Understanding hydraulic fracture stimulated horizontal Eagle Ford completions, SPE/EAGE European Unconventional Resources Conference & Exhibition-From Potential to Production March 20–22, 2012, Vienna, Austria. https://doi.org/10.2118/152533-MS.
[40] Thomas Ewing, TEXAS THROUGH TIME' - LONE STAR GEOLOGY FOR GENERAL AUDIENCES, 2016, https://doi.org/10.1130/abs/2016SC-273889.
[41] EIA, Permian Basin Wolfcamp and Bone Spring Shale Plays Geology Review, U.S. Energy Information Administration, 2019. https://www.eia.gov/maps/pdf/Wolfcamp BoneSpring EIA Report July2019.pdf.
[42] S.C. Ruppel, Anatomy of a Paleozoic basin: the Permian Basin, USA: introduction, overview, and evolution, in: S.C. Ruppel (Ed.), Anatomy of a Paleozoic Basin: the Permian Basin, USA (Vol. 1, Ch. 1): the University of Texas at Austin, Bureau of Economic Geology Report of Investigations 285; AAPG Memoir 118, 2019, pp. 1–27.
[43] U.S. Department of Energy, Modern shale gas development in the United States: a primer. https://www.energy.gov/fecm/downloads/modern-shale-gas-development-united-states-primer, 2009.
[44] D.K. Higley, M.E. Henry, M.D. Lewan, J.K. Pitman, The New Albany Shale Petroleum System, Illinois Basin - Data and Map Image Archive from the Material-Balance Assessment, 2003, https://doi.org/10.3133/ofr200337.
[45] N.R. Hasenmueller, J.B. Comer, GIS Compilation of Gas Potential of the New Albany Shale in the Illinois Basin, Gas Research Institute, Chicago, Ill, 2000.
[46] N.A. Azzolina, D.V. Nakles, C.D. Gorecki, W.D. Peck, S.C. Ayash, L.S. Melzer, S. Chatterjee, CO_2 storage associated with CO_2 enhanced oil recovery: a statistical analysis of historical operations, Int. J. Greenh. Gas Control 37 (2015) 384–397.
[47] Torres, Jose A., Jin, Lu, Bosshart, Nicholas W., Pekot, Lawrence J., Sorensen, James A., Peterson, Kyle, Anderson, Parker W., and Steven B. Hawthorne, Multiscale modeling to evaluate the mechanisms controlling CO_2-based enhanced oil recovery and CO_2 storage in the Bakken Formation, Unconventional Resources Technology Conference July 23-25, 2018, Houston, Texas, pp. 2757-2776.
[48] Adsorption, in: Britannica, 2023. https://www.britannica.com/science/adsorption.
[49] Adsorption, in: Chemistry Dest, 2023. https://chemistry-desk.blogspot.com/2012/10/adsorption.html [25 Jan.2023].
[50] Li, Yinghui, and Hui Pu, Modeling Study on CO2 Capture and Storage in Organic-Rich Shale, Carbon Management Technology Conference 17-19 November, 2015, Sugar Land, Texas. doi: https://doi.org/10.7122/439561-MS.
[51] Faye Liu, K. Ellett, Y. Xiao, J.A. Rupp, Assessing the feasibility of CO_2 storage in the New Albany Shale (Devonian–Mississippian) with potential enhanced gas recovery using reservoir simulation, Int. J. Greenh. Gas Control 17 (2013) 111–126.
[52] CMG, Computer Modeling Group, User's Guide – GEM, CNG, Calgary, Alberta, Canada, 2009.
[53] Hall, F.E., Zhou, C., Gasem Jr., K.A.M., Yee, D., Adsorption of Pure Methane, Nitrogen, and Carbon Dioxide and Their Binary Mixtures on Wet Fruitland Coal, Eastern Regional Conference and Exhibition of the Society of Petroleum Engineers: Natural Gas - a Bright Future 8-10 November, 1994, (Charleston, WV, United States).
[54] R. Lenormand, C. Zarcone, A. Sarr, Mechanisms of the displacement of one fluid by another in a network of capillary ducts, J. Fluid Mech. 135 (1983) 337–353.
[55] S.C. Krevor, R. Pini, B. Li, S.M. Benson, Capillary heterogeneity trapping of CO_2 in a sandstone rock at reservoir conditions, Geophys. Res. Lett. 38 (15) (2011).
[56] R. Juanes, E.J. Spiteri, F.M. Orr Jr., M.J. Blunt, Impact of relative permeability hysteresis on geological CO_2 storage, Water Resour. Res. 42 (12) (2006).
[57] C.S. Land, Calculation of imbibition relative permeability for two-and three-phase flow from rock properties, Soc. Petrol. Eng. J. 8 (2) (1968) 149–156.
[58] W. Stumm, J.J. Morgan, Aquatic Chemistry: Chemical Equilibria and Rates in Natural Waters, Wiley, New York, 1996.
[59] Y.K. Li, L.X. Nghiem, Phase equilibria of oil, gas and water/brine mixtures from a cubic equation of state and Henry's law, Can. J. Chem. Eng. 64 (3) (1986) 486–496.
[60] R.J. Bakker, Package FLUIDS 1. Computer programs for analysis of fluid inclusion data and for modelling bulk fluid properties, Chem. Geol. 194 (2003) 3–23.
[61] Zhiming Chen, Xinwei Liao, Xiaoliang Zhao, Xiangji Dou, Langtao Zhu, Development of a trilinear-flow model for carbon sequestration in depleted shale, SPE J. 21 (2016) 1386–1399, https://doi.org/10.2118/176153-PA.
[62] K. Malek, M.O. Coppens, Knudsen self- and Fickian, Diffusion in rough nanoporous media, J. Chem. Phys. 119 (5) (2003) 2801–2811.
[63] Q. Chen, Q. Liu, Z. Tao, Study on the mechanism of rock stress sensitivity using a random pore network simulation, J. Chem. 2016 (2016) 1–10.
[64] Pedrosa, O.A., Pressure transient response in stress-sensitive formations, In SPE California Regional Meeting 2–4 April, 1986, Oakland, California. doi: https://doi.org/10.2118/15115-MS.

[65] H. Mukherjee, M.J. Economides, A parametric comparison of horizontal and vertical well performance, SPE Form. Eval. 6 (2) (1991) 209–216.
[66] Qin He, Teresa Reid, Guofang Zheng, Reservoir simulation of CO_2 sequestration in shale reservoir, SPE Eastern Regional Meeting 2–3 November, 2021, Farmington, Pennsylvania, USA.
[67] R.I. Masel, Principles of Adsorption and Reaction on Solid Surfaces, 1996.
[68] Sai Wang, Kouqi Liu, Juan Han, Kegang Ling, Hongsheng Wang, Investigation of properties alternation during super-critical CO_2 injection in shale, Appl. Sci. 9 (8) (2019) 1686, https://doi.org/10.3390/app9081686.
[69] Patil, Parimal A., Chidambaram, Prasanna, Bin Ebining Amir, M Syafeeq, Tiwari, Pankaj K., Das, Debasis P., Picha, Mahesh S., B A Hamid, M Khaidhir, and Raj Deo Tewari, FEP Based Model Development for Assessing Well Integrity Risk Related to CO2 Storage in Central Luconia Gas Fields in Sarawak, International Petroleum Technology Conference 23 March–1 April, 2021, Virtual. doi: https://doi.org/10.2523/IPTC-21472-MS.
[70] Widyanita, Ana, and W Ahmad B W Zairudin, Advanced Analysis of CO2 Storage Development Plan and its Unique Compared to Field Development Plan, Abu Dhabi International Petroleum Exhibition & Conference 9-12 November, 2020, Abu Dhabi, UAE. doi: https://doi.org/10.2118/202794-MS.